Available online at www.sciencedirect.com
SCIENCE DIRECT®
Combustion and Flame 145 (2006) 765–778
Combustion and Flame
www.elsevier.com/locate/combustflame

Soot formation and temperature field structure in laminar propane–air diffusion flames at elevated pressures

Décio S. Bento [a], Kevin A. Thomson [b], Ömer L. Gülder [a,*]

[a] *Institute for Aerospace Studies, University of Toronto, 4925 Dufferin Street, Toronto, ON M3H 5T6, Canada*
[b] *National Research Council, ICPET Combustion Technology, 1200 Montreal Road M-9, Ontario K1A 0R6, Canada*

Received 1 March 2005; received in revised form 30 January 2006; accepted 31 January 2006

Available online 6 March 2006

Abstract

The effect of pressure on soot formation and the structure of the temperature field was studied in coflow propane–air laminar diffusion flames over the pressure range of 0.1 to 0.73 MPa in a high-pressure combustion chamber. The fuel flow rate was selected so that the soot was completely oxidized within the visible flame and the flame was stable at all pressures. Spectral soot emission was used to measure radially resolved soot volume fraction and soot temperature as a function of pressure. Additional soot volume fraction measurements were made at selected heights using line-of-sight light attenuation. Soot concentration values from these two techniques agreed to within 30% and both methods exhibited similar trends in the spatial distribution of soot concentration. Maximum line-of-sight soot concentration along the flame centerline scaled with pressure; the pressure exponent was about 1.4 for pressures between 0.2 and 0.73 MPa. Peak carbon conversion to soot, defined as the percentage of fuel carbon content converted to soot, also followed a power-law dependence on pressure, where the pressure exponent was near to unity for pressures between 0.2 and 0.73 MPa. Soot temperature measurements indicated that the overall temperatures decreased with increasing pressure; however, the temperature gradients increased with increasing pressure.

Keywords: Soot formation; High pressure; Laminar diffusion flame

1. Introduction

The details of the chemical and physical mechanisms of soot formation processes in combustion remain uncertain due to the highly complex nature of hydrocarbon flames. The mechanisms of soot formation have been investigated extensively over many years and only very broad features of the formation processes have been established. In addition to great uncertainty regarding formation mechanisms (see, for example, Krestinin [1]), the control and prediction of soot levels in practical combustion devices are further impeded by the complexities introduced by the transient operating conditions, existence of a nonhomogeneous and turbulent flow field, and the chemistry of distillate fuels consisting of several hundred hydrocarbon compounds. One of the important parameters in soot formation is pressure. Current understanding

* Corresponding author. Fax: +1 416 667 7799.
E-mail address: ogulder@utias.utoronto.ca (Ö.L. Gülder).

0010-2180/$ – see front matter
doi:10.1016/j.combustflame.2006.01.010

of the influence of pressure on soot formation and oxidation is very sketchy, although the majority of practical combustion devices operate at elevated pressures.

Although most of the diffusion flames in practical combustion systems and fires are essentially turbulent, detailed direct study of these flames is not always tractable because of the intermittency and the short residence times involved [2]. However, known similarities in laminar and turbulent diffusion flames, which are exploited for simplified analysis of turbulent flames using laminar flamelet concepts, justify the study of laminar diffusion flames that provide a tractable flame model (see, for example, Moss [3], Cavaliere and Ragucci [4]). For this reason the more easily controlled laboratory experiments are performed in laminar diffusion flames and shock tubes. One disadvantage of the shock tubes is that they have a very short residence time as compared to practical flames.

Three types of laminar diffusion flame burners are commonly used by soot researchers: the coflow, counterflow, and Wolfhard–Parker burners. Although the counterflow (opposed jet) and Wolfhard–Parker burners produce almost one-dimensional flames, they may suffer from stability problems at elevated pressures. In addition, in counterflow burner flames the stagnation point location is very critical and it can vary with the choice of flow conditions. Coflow burner flames are radially axisymmetric two-dimensional flames with demonstrated stability at high pressures [5,6]. A significant portion of research work on soot formation and oxidation has been conducted on coflow laminar diffusion flames.

Research efforts related to soot formation in laminar diffusion flames at high pressures are limited to very few studies. Flower and Bowman [7] studied laminar diffusion flames of ethylene at a pressure range of 0.1 to 1 MPa by measuring line-of-sight integrated soot volume fractions and temperatures along the flame centerline. They report a pressure scaling of soot maximum integrated volume fraction with an exponent of 1.2 ± 0.1 from atmospheric to 1 MPa pressure for ethylene diffusion flames. Measurements of Lee and Na [8] indicate similar pressure scaling for the maximum integrated soot volume fraction with an exponent of 1.26 in laminar ethylene flames from atmospheric to 0.4 MPa. The data reported by Lee and Na [8] also imply a square dependence on pressure of maximum local soot volume fraction at a height of 20 mm above the burner rim [6]. McCrain and Roberts [9] measured path-integrated and local soot volume fractions by line-of-sight attenuation and laser-induced incandescence, respectively. Their measurements covered a pressure range of 0.1 to 2.5 MPa in methane flames and 0.1 to 1.6 MPa in ethylene diffusion flames. Thomson et al. [6] reported radially resolved soot concentration and soot temperature measurements, which are the first detailed data sets on soot and temperature at elevated pressures up to 4 MPa, in laminar diffusion flames of methane using soot emission spectroscopy and line-of-sight attenuation. It was shown that in high-pressure laminar diffusion flames, the fraction of fuel carbon content that is converted to soot, rather than the line-of-sight integrated volume fraction, should be used in assessing the sensitivity of soot formation to pressure [6,7]. The results of these four studies are summarized in Table 1. Although a significant portion of combustion devices that operate at high pressures use liquid fuels, there are no reported measurements of sooting behavior of liquid fuels in laminar diffusion flames at pressures higher than atmospheric.

Most of the soot studies at atmospheric pressure are done with ethylene diffusion flames, and to a certain extent with acetylene and methane flames. Although ethylene is not a common fuel used in combustion devices, it is one of the most common olefins as an intermediate species in hydrocarbon combustion and pyrolysis. Acetylene is assumed to play a major role in soot inception and growth in hydrocarbon combustion and pyrolysis. Although methane is the most common gaseous fuel (natural gas), it behaves very much differently than the rest of the hydrocarbons; it is not a typical hydrocarbon and information obtained with methane may not be fully applicable to other hydrocarbons. High-pressure soot studies reported in the literature are limited to measurements on ethylene and methane flames, Table 1. Propane, on the other hand, mimics higher hydrocarbons to a certain extent and measurements with propane may have some relevance to liquid hydrocarbon fuels. For this reason, the sooting behavior of propane at elevated pressures is of interest.

Information on soot formation processes in laminar diffusion flames at higher pressures is limited to ethylene and methane flames, and detailed measurements of soot and temperature are available only for methane. The main objective of the research reported in this paper is to determine spatially resolved soot volume fraction and temperature in coflow propane–air laminar diffusion flames at elevated pressures. Spectral soot emission (SSE) and limited line-of-sight attenuation (LOSA) measurements (for comparison to SSE) in the propane flame are presented for pressures from atmospheric to 0.73 MPa. The higher pressure limit was set by the fact that propane liquefies above this pressure. The results reported here extend the available information on sooting tendency as a function of pressure to propane diffusion flames.

Table 1
Summary of previous experimental results and results of the current study on the pressure dependence of soot in laminar diffusion flames

Refs.	Pressure range [MPa]	Fuel and fuel flow rate [mg/s]	Pressure exponent n in [soot] $\propto P^n$		
			Path integrated maximum soot	Local maximum soot (location)	Fraction of fuel's carbon converted to soot
[7]	0.1–1	Ethylene 1.9, 2.7, and 4.4	1.2 ± 0.1		
[8]	0.1–0.4	Ethylene 3.4	1.26	2 (20 mm above burner rim)	
[9]	0.1–1.6	Ethylene 1.13	1.2	1.7	
[9]	0.1–2.5	Methane 1.1	1	1.2	
[6]	0.5–2	Methane 0.55	1.3	2	1
[6]	2–4	Methane 0.55	0.9	1.2	0.1
This work	0.1–0.2	Propane 0.49	3.4[a]		3.3[a]
This work	0.2–0.73	Propane 0.49	1.4	1.8	1.1

[a] See text for cautionary remarks about the values of these exponents.

2. Experimental methodology

The experimental high-pressure combustion chamber and the laminar diffusion flame burner used in this study are described in detail in [6]. The design pressure of the chamber is about 10 MPa, and its internal diameter and internal height are 0.24 and 0.6 m, respectively. Optical access into the chamber is through three ports at 0°, 90°, and 180° locations, allowing line-of-sight measurements as well as 90° scattering and imaging experiments. A schematic of the chamber is shown in Fig. 1. The laminar diffusion flame burner used in this work was based on a design by Miller and Maahs [5], who achieved a stable flame over a pressure range of 0.1 to 5 MPa by placing a circular quartz chimney around the flame. The burner has a fuel nozzle exit diameter of 3.06 mm and an air nozzle diameter of 25 mm. Sintered metal-foam elements (80 pores per inch) are included in the fuel and air nozzles to straighten and reduce instabilities in the flow and to create a top-hat exit velocity profile as the gases leave the foam elements. A tapered fuel nozzle reduces recirculation from the burner tip and improves stability of the fluid–ambient interface [5]. In the original design [5], a cylindrical quartz tube surrounded the flame to aid flame stabilization. For the present experiments, the quartz tube was replaced by a new chimney designed to include three flat windows aligned with the three viewing ports on the chamber. The flame is ignited using a glow plug incorporated into the chimney and located above the flame.

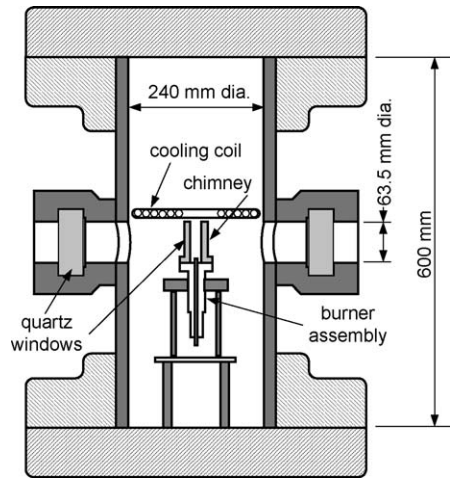

Fig. 1. A schematic of the high-pressure combustion chamber with a design pressure of about 10 MPa.

The diffusion flame burner and the chimney design provided stable flames with methane up to 8 MPa, which was reported previously [6], and with propane at all pressures considered in this work. Flames exhibited long-term stability for all pressures with an rms flicker of the flame on the order of 0.1 mm. This level of flame movements was considered as satisfactory for reliable measurements. However, it was noted that propane flames were not as stable as the methane flames we studied on the same rig previously [6].

To allow comparison of results for different pressures, it is important to maintain similar reference

conditions. To achieve this, a constant fuel mass-flow rate was maintained at all pressures, thus allowing constant carbon release from the nozzle based on the fuel's chemical composition. It is also important to view the progression of the soot formation and destruction at similar residence times. Theoretical analysis suggests that the height of a constant mass-flow rate diffusion flame of a circular burner is invariant with pressure [10]. This prediction is approximately true over the pressure range studied [6].

The theory and overall experimental layout of the spectral soot emission diagnostic (SSE) are described elsewhere [11]. In SSE, line-of-sight radiation emission from soot is measured along chords through the flame. A series of emission projections at a given height in the flame can be inverted to obtain radially resolved emission rates, from which temperature and soot volume fraction can be determined when soot optical properties are known. For the current measurements a 300-mm focal length lens (f/45, 2:1 magnification) is used to image the object plane at burner center onto a vertical entrance slit (height 0.5 mm, width 0.025 mm) of a spectrometer. Output from the spectrometer is imaged onto a 16-bit CCD detector (1100 × 330 pixels), Fig. 2. Knife-edge scans across a diffuse light source located at the object plane show a horizontal spatial resolution of 50 μm. The system is calibrated for radiation intensity using a filament lamp, with a calibration traceable to NIST, placed inside the chamber. The uncertainty in the spectral radiance temperature is about 5 K. Soot emission is measured over a wavelength range of 690–945 nm. Spectra are averaged over the vertical height of the entrance slit as well as across 21-nm spectral widths, thus providing 12 spectral data points per line-of-sight acquisition. One-dimensional tomography is applied to each wavelength range using a three-point Abel inversion method [12]. Local temperatures are determined from the spectral shape of the inverted soot emission intensity. Soot volume fraction is then determined from the soot emission intensity using the measured temperatures. The soot refractive index function, $E(m)$, is assumed to be constant and equal to 0.274 for the calculations. This assumption is consistent with results of Krishnan et al. [13]. Sensitivity of SSE results to $E(m)$ is discussed briefly in Section 4. Modeling of the flame emission using the methods described in [11] shows that emission attenuation by soot introduces only a small error (<2%) into the measurements for even the highest soot loadings observed in this flame. Therefore no attenuation correction is applied.

The line-of-sight attenuation (LOSA) diagnostic is a simplified version of the 2D LOSA diagnostic described in [14]. In LOSA, a line-of-sight measurement of the intensity of a small light beam transmitted

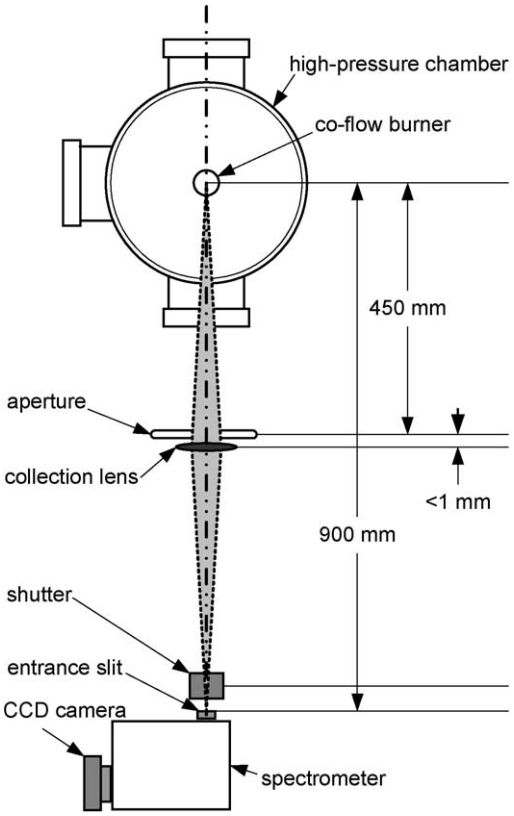

Fig. 2. The layout of the soot spectral emission measurement system.

through a flame is made. When divided by a measurement of the intensity of the beam transmitted along the same path without the flame present, the transmissivity of the flame along the chord can be determined. A series of transmissivity measurements at a given height in the flame can be inverted to obtain radially resolved extinction coefficients from which soot volume fraction can be determined. The optical layout for the LOSA measurements is given in [6]. Light from a mercury arc lamp is first focused onto a 50-μm pinhole. Light transmitted through the pinhole is modulated using a chopper wheel and imaged at the center plane of the burner with a 1.5:1 demagnification at a speed of f/19. Knife-edge scans of the lamp beam at burner center show the beam width to be less than 40 μm across the diameter of the burner nozzle. A collection lens downstream of the burner refocuses the transmitted lamp light onto a photodiode detector coupled to a lock-in amplifier. The collection lens is large (i.e., 100 mm diam.) to accommodate beam steering of the light transmitted through the flame, which becomes quite pronounced elevated pressures. A glass plate located between the imaging lens and chamber reflects a portion of the lamp light onto a second photodiode which is used to ratio out

temporal variation in the lamp intensity. Both photodiodes are filtered with 830 nm narrow band filters. For each measurement height, two scans are required, one with the flame lit and the second with the flame extinguished. The method used to calculate soot volume fraction measurements from line-of-sight transmissivity measurements is described in [14].

Measurements of soot volume fraction and temperature were obtained using SSE for pressures 0.1, 0.2, 0.4, 0.6, and 0.73 MPa. Limited soot measurements were done using LOSA for comparison to SSE measurements. Constant mass flow rates of propane and air of 0.49 mg/s and 0.4 g/s, respectively, were maintained at all pressures. For each pressure, measurements were obtained at height increments of 0.5 mm from the base to the tip of the flame and at horizontal increments of 50 μm.

3. Results and discussion

Visible flame heights, as indicated by soot radiation (that is, by the presence of any soot), varied moderately by about 10% over the entire pressure range and remained constant at approximately 9.5 mm between 0.4 and 0.73 MPa. For pressures lower than 0.4 MPa, visible flame heights tended to decrease slightly and the blue premixed region near the nozzle exit became more expansive as the pressure neared atmospheric pressure. Soot formation seemed to occur mainly at the tip of the flame at lower pressures and as the pressure increased, the luminous carbon zone moved downward, filling an increasingly large portion of the flame as also noted by Miller and Maahs [5] and Thomson et al. [6].

Along with moderate flame height variation, axial flame diameters varied considerably over the entire pressure range studied. Below 0.4 MPa, the blue premixed region adjacent to the nozzle exit had a bulbous appearance and was wider than the exit diameter of the burner nozzle. In the luminous region above the premixed region, the axial flame diameters converged quickly to the flame tip. As the pressure was increased, axial flame diameters decreased, giving an overall stretched appearance to the flame as noted by Flower and Bowman [7] and Thomson et al. [6]. Between 0.2 and 0.73 MPa pressure, the cross-sectional area of the flame (measured from the radius defined by the outer edges of the sooting region at each measurement height) showed an inverse dependence on pressure, in agreement with the data of Thomson et al. [6] and McCrain and Roberts [9], although Glassman [15] reports an inverse square-root dependence on pressure. An inverse dependence of the flame cross-sectional area on pressure implies that the residence times are independent of the pressure and measurements can be compared at the same heights above the burner exit.

This can be illustrated simply as follows: It is shown that, to a first approximation, the height of a buoyancy-dominated laminar coflow diffusion flame, established on a circular fuel nozzle, scales with molecular diffusivity, D, and fuel flow rate, Q, as [10,15]

$$H \propto \frac{Q}{D} \propto \frac{1}{P}\frac{\nu A}{D} \tag{1}$$

for a fixed flow rate of fuel. Here, ν is the mean fuel exit velocity and A is the fuel nozzle exit area. Since molecular diffusivity, D, is inversely propor-

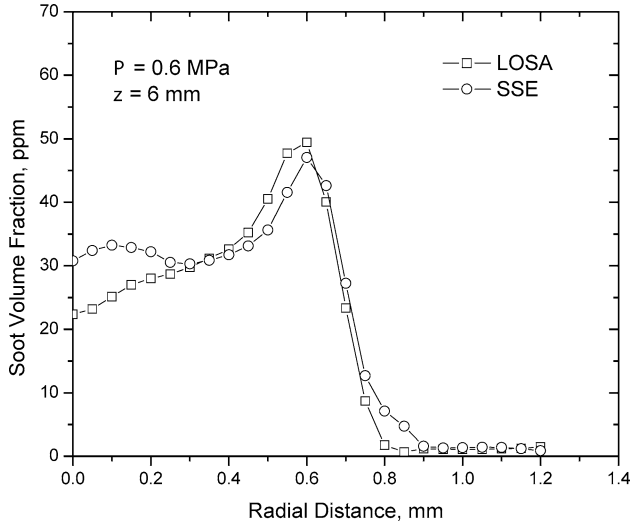

Fig. 3. Comparison of soot concentrations measured with two methods at a pressure of 0.6 MPa and height of 6 mm above the burner exit.

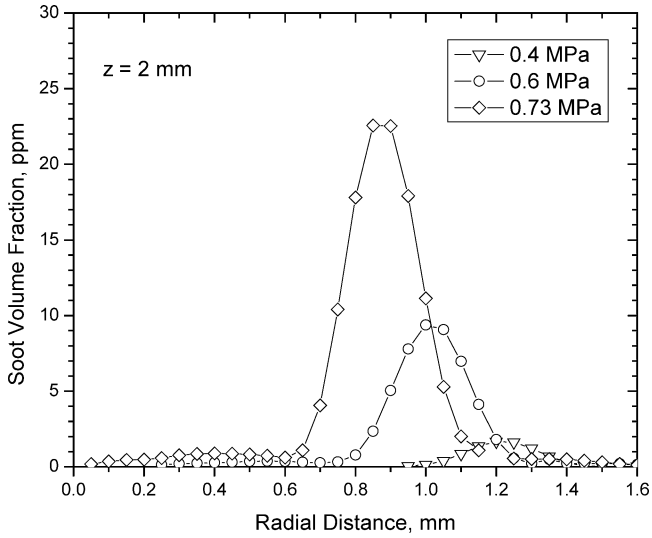

Fig. 4. Soot concentration profiles measured by SSE at height 2 mm above the burner exit at $P = 0.4$, 0.6, and 0.73 MPa.

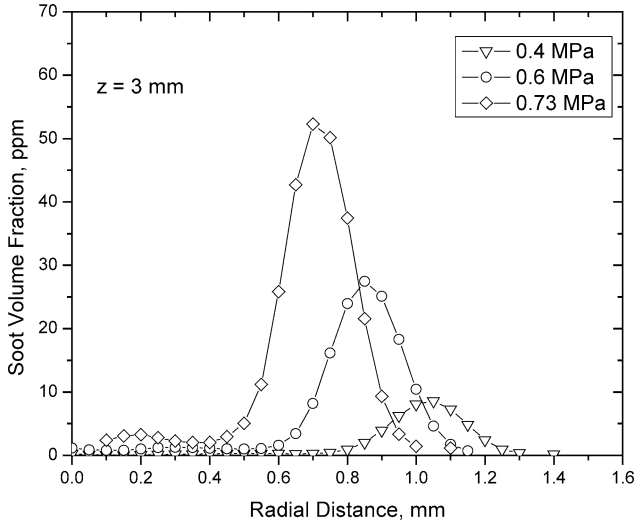

Fig. 5. Soot concentration profiles measured by SSE at height 3 mm above the burner exit at $P = 0.4$, 0.6, and 0.73 MPa.

tional to pressure, P, i.e., $D \propto 1/P$, the height of the diffusion flame is independent of the pressure. At a given height above the burner nozzle exit, the average velocity within the flame envelope will not change with pressure if the flame cross-sectional area varies inversely with pressure. That is, as the pressure increases, the material flow within the flame envelope will be through a narrower cross-section but at a higher density, thus keeping the average velocity constant at a given height. This argument assumes that the air entrainment into the flame envelope does not change much with pressure.

For comparison, the soot volume fraction profiles obtained using both SSE and LOSA soot diagnostics at $P = 6$ atm and $z = 6$ mm are shown in Fig. 3. Radial profiles of soot volume fraction collected using SSE and LOSA were quite consistent, differing by a maximum of about 30%. Also, peak soot locations occurred at equal radial positions and peak soot volume fractions differed by about 5%. Thomson et al. [6] report differences by at most 30% in their study with methane flames. However, larger discrepancies were encountered near the core of the flame [6], a region where SSE has limited accuracy due to the low levels of soot relative to the peak soot volume fraction. A detailed discussion of the comparison of LOSA and SSE is given in [6].

In Figs. 4–10, soot concentration profiles measured by SSE are shown at heights of 2 mm to 8 mm. Measurements were made by scanning the en-

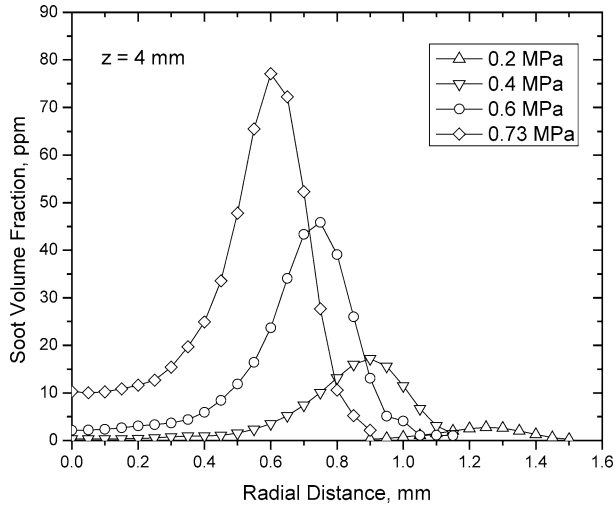

Fig. 6. Soot concentration profiles measured by SSE at height 4 mm above the burner exit at $P = 0.2$, 0.4, 0.6, and 0.73 MPa.

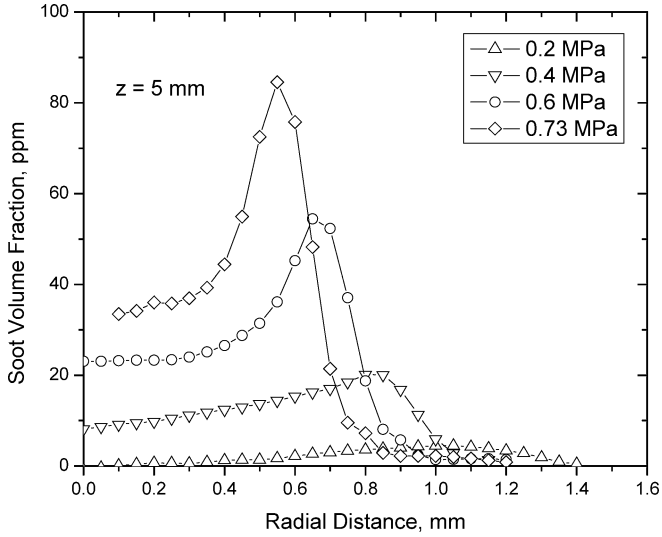

Fig. 7. Soot concentration profiles measured by SSE at height 5 mm above the burner exit at $P = 0.2$, 0.4, 0.6, and 0.73 MPa.

tire flame diameter at each measurement height; however, the data shown in Figs. 4–10 represent averages of the left- and right-side scans. The soot forms first in an annular band near the burner rim, much like the atmospheric laminar diffusion flames. Near the mid-height of the flame, the annular distribution of soot remains pronounced, but soot also begins to appear in the core of the flame. At the tip of the flame, the annular distribution disappears and a peak soot concentration is observed on the flame centerline, Fig. 10. The contraction of the flame diameter with pressure is reflected in the location of the peaks in the radial profiles of soot volume fraction, Figs. 4–10. Soot concentrations showed a significant increase with pressure; the peak soot volume fraction increased from about 0.5 ppm at atmospheric pressure to over 80 ppm at 0.73 MPa (Fig. 7).

Flower and Bowman [7], Lee and Na [8], and McCrain and Roberts [9] report path-integrated (line-of-sight) soot volume fractions versus pressure to assess the pressure sensitivity of soot formation. To compare the current results with previous work [7–9], line integrals of the soot concentration profiles were calculated. Line-of-sight integrated soot concentration profiles along the flame centerline at elevated pressures are similar to those observed at atmospheric flames, Fig. 11. The line-of-sight integrated soot volume fractions scale with pressure [7–9] as

$$f_{v_{\text{line}}} = \int f_v(r)\,\mathrm{d}r \propto P^n, \tag{2}$$

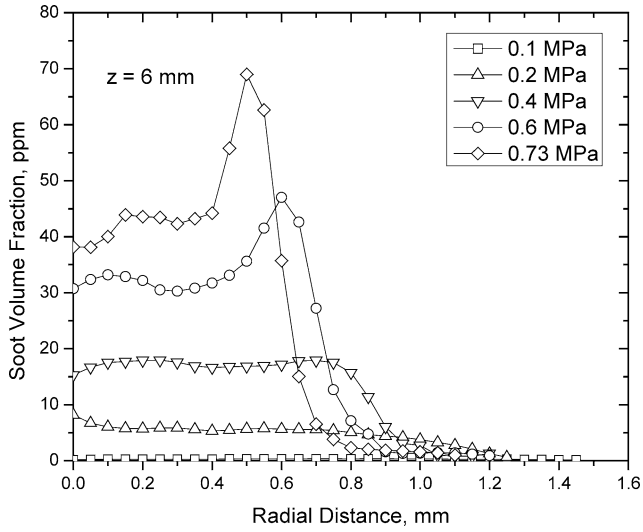

Fig. 8. Soot concentration profiles measured by SSE at height 6 mm above the burner exit at $P = 0.1$, 0.2, 0.4, 0.6, and 0.73 MPa.

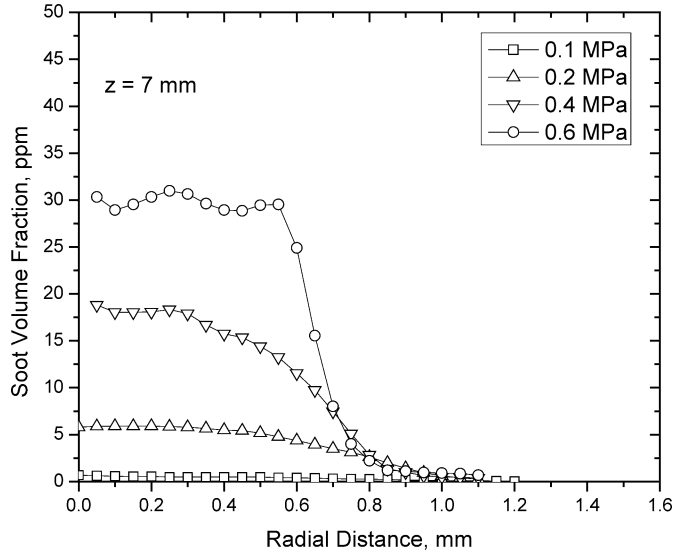

Fig. 9. Soot concentration profiles measured by SSE at height 7 mm above the burner exit at $P = 0.1$, 0.2, 0.4, and 0.6 MPa.

where n values are listed in Table 1. The maximum line-of-sight soot volume fractions, i.e., the peak values of the profiles in Fig. 11, were fitted to Eq. (2) to estimate the value of n for the present measurements with propane. The value of the exponent n is about 1.4 for the pressure range from 0.2 to 0.73 MPa, Fig. 12. This value of exponent n is slightly larger than the exponents reported previously for ethylene and methane, Table 1. To account for the increase in soot concentration between 0.1 and 0.2 MPa, the pressure exponent should be about 3.4, Fig. 11. This is a very steep change in soot concentration with pressure and requires further measurements for confirmation.

Maximum soot volume fraction shows a dependence on pressure, with a pressure exponent of about 1.8 between 0.2 and 0.73 MPa. This value is comparable to exponents reported for methane [6] and ethylene [8,9], but higher than the exponent reported in [9] for methane, Table 1.

As expected, soot volume fraction increases with increasing pressure, since the flame is narrowing, suggesting that all species are at higher concentration. To assess the sensitivity of sooting propensity of the flame to pressure, Thomson et al. [6] propose that the percentage of total carbon in the fuel converted to soot as a function of height is a better measure than the maximum line-of-sight integrated soot con-

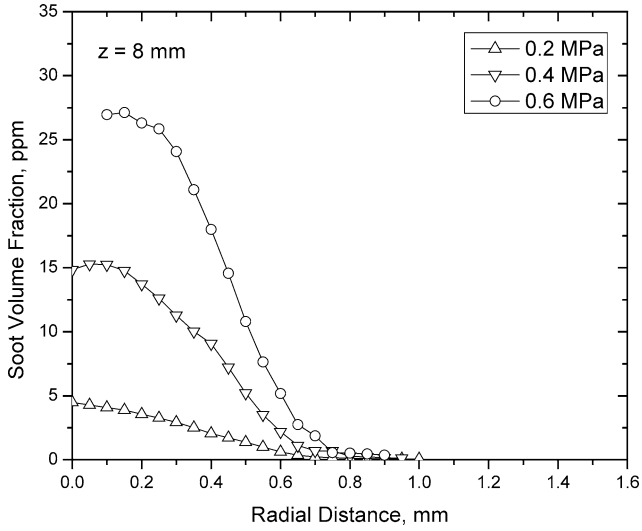

Fig. 10. Soot concentration profiles measured by SSE at height 8 mm above the burner exit at $P = 0.2$, 0.4, and 0.6 MPa.

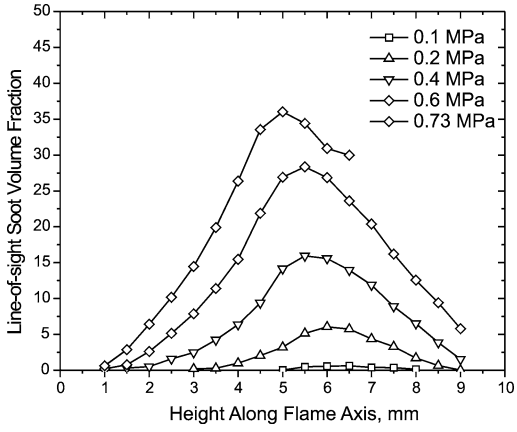

Fig. 11. Line-of-sight average soot volume fraction along the flame centerline.

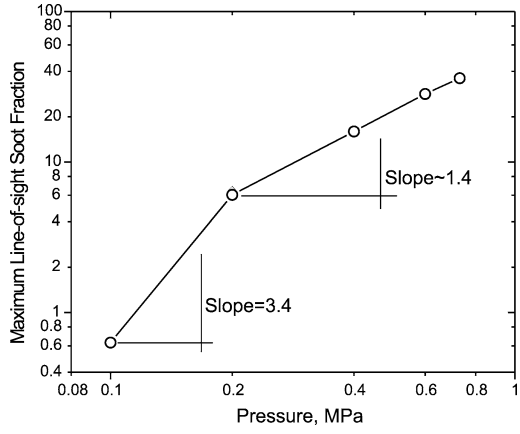

Fig. 12. Maximum line-of-sight averaged soot volume fraction as a function of pressure.

centrations. We use the same approach to assess the influence of pressure. The mass flow rate of carbon, in the form of soot, can be determined through the relationship

$$\dot{m}_s(z) = v_z(z)\rho_s \int 2\pi r f_v(r, z)\, dr, \tag{3}$$

where v_z is the axial velocity, $\rho_s = 1.8$ g/cm^3 is the soot density, and z is the axial height. The axial velocity is estimated using the relationship $v_z(z) = \sqrt{2az}$, where a is an acceleration constant commonly assumed to be 25 m/s^2 [7,10]. The percentage of carbon in the fuel converted to soot is simply $\eta_s = \dot{m}_s/\dot{m}_c$, where $\dot{m}_c$ is the carbon mass flow rate at the nozzle exit. The results of this calculation are plotted in Fig. 13. Peak carbon conversion occurs about 6 mm above the burner nozzle at a pressure of 0.1 MPa, 5.5 mm for pressures of 0.2 and 0.4 MPa, and 5 mm for pressures of 0.6 and 0.73 MPa, Fig. 13. Up to the point of peak carbon conversion, the curves of carbon conversion with height are approximately linear and the slopes increase with increasing pressure.

A plot of maximum percentage conversion of carbon to soot as a function of pressure is shown in Fig. 14. It was observed that $\eta_s \propto P^n$, where $n = 3.3$ for pressures ranging between 0.1 and 0.2 MPa and $n = 1.1$ for the pressure range of 0.2 to 0.73 MPa. Thus even when the impact of flame narrowing is accounted for, it was shown that soot formation is enhanced by pressure. However, at pressures between 0.1 and 0.2 MPa, the sensitivity shown in Fig. 14 seems very high, and further measurements are needed to verify the observed sensitivity to pres-

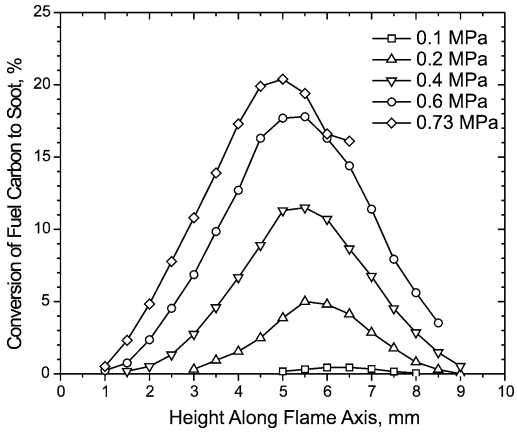

Fig. 13. Percentage conversion of carbon from fuel to soot as a function of axial location along the flame axis.

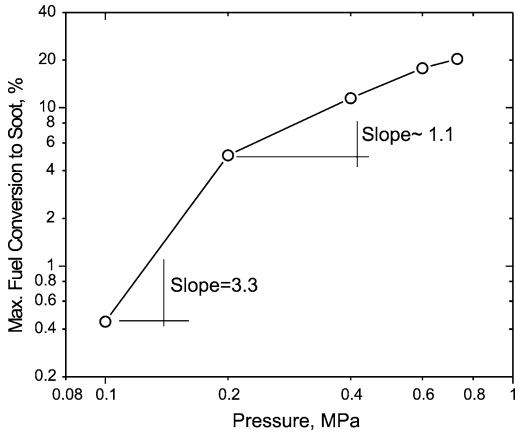

Fig. 14. Maximum percentage conversion of carbon from fuel to soot as a function of pressure.

sure from atmospheric to 0.2 MPa. The pressure exponent $n = 1.1$ obtained for propane diffusion flames is very close to $n = 1$ reported for methane flames in the range of 0.5 to 2 MPa [6]. One interesting result reported in [6] with methane diffusion flames is that the pressure exponent decreases sharply to 0.1 when the pressure exceeds 2 MPa. It was not possible to go to pressures similar to those in [6] with the current experimental rig (without modifications to the burner and fuel feeding system) due to thermophysical properties of propane.

In this propane diffusion flame, the carbon conversion to soot peaked at about 20% at 0.73 MPa compared to 40–50% observed by Flower and Bowman in an ethylene flame [7] and about 5% reported by Thomson et al. [6] in a methane flame, both at 1 MPa. It should be noted that in [7], the high conversion to soot is not due only to the fuel type but was contributed by the higher mass-flow rates of ethylene as well.

Measured soot temperature profiles are shown in Fig. 15 at heights 2 to 9 mm, with 1-mm intervals, above the burner exit. Since SSE data are based on measurements of soot emission, temperatures can only be determined in locations where sufficient soot exists to provide a resolvable signal. This typically occurs at radial locations centered about the zones of peak soot volume fraction. From previous characterization of the SSE diagnostic [11], temperatures are known to decrease at the outer edges of the annuli earlier than would be predicted by flame models or other experimental diagnostics, thus underpredicting the peak temperature in the reaction zone. It is believed that this fall-off is caused by errors introduced through the inversion algorithm when the rapidly decreasing line-of-sight emission intensities at the edge of the flame are inverted. In the core of the flame, temperatures can also be inaccurate when soot volume fractions are low relative to peak soot volume fractions in the annulus [6]. Consequently, the temperature plots provided here have been limited to regions centered about the soot annuli. This is justified by the fact that the agreement between soot volume fraction measurements using SSE and LOSA in these regions is good and requires accurate estimation of the soot temperature. The radial temperature profiles are qualitatively similar to those observed in atmospheric-pressure diffusion flames [11,16]. It is believed that the increased uncertainties in temperature in the core of the flame and on the outside of the soot annulus may be linked to optical limitations and beam steering when the SSE diagnostic is applied in such a narrow flame. The greatest disagreement between LOSA and SSE measurements is observed in the core of the flame [6,17,18]. Here, the uncertainty in temperature measurements limits the accuracy of the SSE soot volume fraction measurements. Multiple measurements at the same location at different times showed that the temperature curves are repeatable, within 2%, including any anomalous temperature values discussed above [6].

The temperature plots in Fig. 15 show steep radial temperature gradients across the soot annulus and a general axial increase in temperature. The rate of temperature increase with axial position increases with increasing pressure; however, the overall temperature drops with increasing pressure, most significantly in the lower half of the flame. As the pressure increases, the visible flame gets narrower resulting in steeper radial temperature gradients. Maximum temperature gradients along the flame axis, calculated from the temperature profiles, are shown in Fig. 16. The gradients are the highest near to the burner rim, and they generally decrease with increasing height. There seems to be a local maximum around height 4–5 mm, which was also observed in methane flames [6]. The

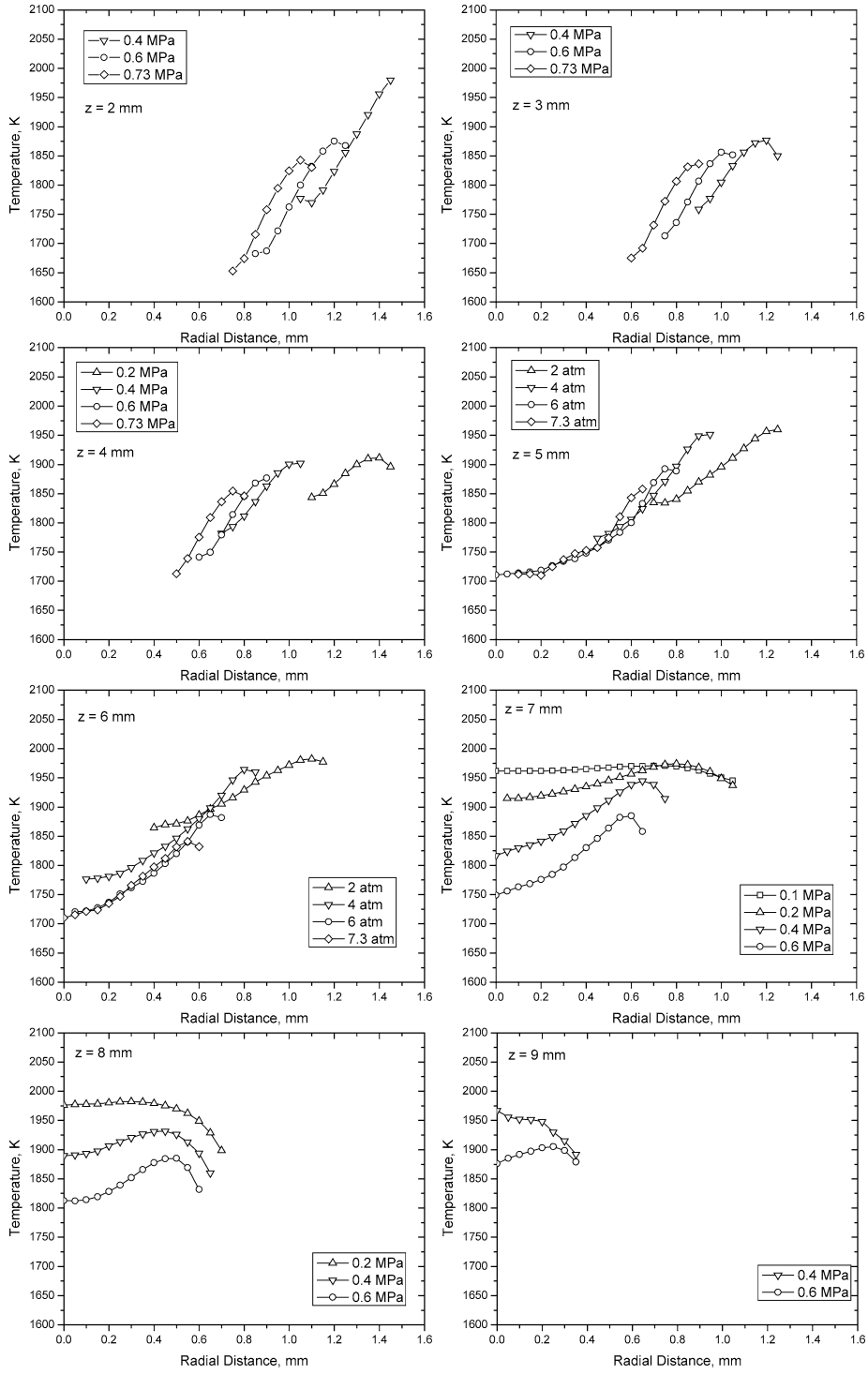

Fig. 15. Soot temperature profiles at heights from 2 to 9 mm above the burner exit at various pressures.

radial temperature gradients generally increase at all heights with pressure, except at the highest pressure at heights above 5 mm. Near the burner nozzle, radial temperature gradients are as high as 800–1000 K/mm at the higher pressures, whereas they drop to about 200–400 K/mm around height 7–7.5 mm.

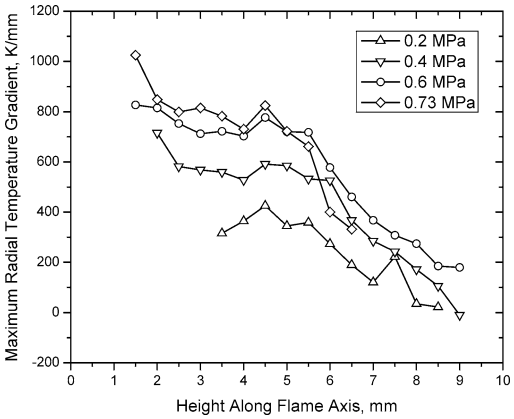

Fig. 16. Maximum radial gradients of soot temperature as a function of axial location along the flame axis at different temperatures.

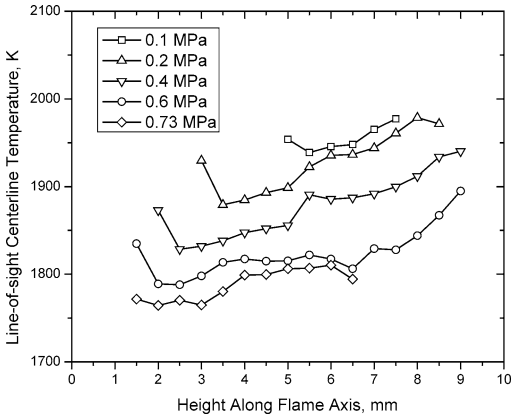

Fig. 17. Line-of-sight emission-averaged soot temperature along the flame axis at different pressures.

Flower [19] reported soot particle temperatures determined from line-of-sight measurements of light emission and extinction by soot particles in laminar diffusion flames of ethylene up to 0.7 MPa. To compare present results to those reported in [19], we calculated the averaged temperatures from line-of-sight emission measurements through the flame centerline as a function of height, Fig. 17. It should be noted that these temperatures, plotted in Fig. 17, represent a soot-concentration-weighted average temperature along a chord through the flame centerline (perpendicular to the flame axis) and should correspond closely to peak soot volume fraction location temperatures. The overall trend of the average temperature profiles in Fig. 17 is in qualitative agreement with the data of [19] for the lower half of the flame height. For the upper half of the flame, the temperatures decrease with increasing height in [19], whereas in Fig. 17 they keep increasing with the flame height. The reason for this discrepancy is that the flames in [19] are smoking flames (except at 0.1 MPa); that is, soot is not completely oxidized within the visible flame envelope and escapes from the tip of the flame. In the current work, flames are below their smoke point conditions at all pressures, and as a result, soot oxidation dominates the upper half of the flame and keeps temperature increasing as the heat is released.

A high-temperature region is observed close to the flame base, similar to data reported in [19]. One of the reasons for this is the preheating of the reactants by the fuel nozzle, which is at a higher temperature as a result of heat transfer from the flame. The average temperatures decrease with pressure as a result of increasing heat loss by radiation from the flame, Fig. 17.

There is a lack of understanding of the dependence of soot optical properties, specifically soot refractive index and consequently the function $E(m)$, on soot temperature, soot aggregate structure, and the wavelength. The results of a limited number of studies on the dependence of refractive index on soot temperature reveal that at typical flame temperatures the dependence is not significant, but from room temperature to flame temperatures the imaginary part of the refractive index may change by 50% [20,21]. A recent comprehensive review [22] shows that a Rayleigh–Debye–Gans polydisperse fractal aggregate approach can properly describe the light scattering from soot aggregates as long as the aggregate fractal dimension is less than 2. This approach assumes that the absorption coefficient of soot does not depend on the extent of aggregation, and there is good evidence that the fractal dimension of the soot aggregates is about 1.8 [23–25]. We assumed, for the purposes of this work, that soot refractive index did not have a significant dependence on temperature or on aggregate size.

Krishnan et al. [13] estimate error in their measurements of $E(m)$ to be between 14 and 24%. A linear regression to the data points over the wavelength range of 488 to 800 nm indicates a nearly horizontal trend line with approximately 5%/μm variation in $E(m)$. During initial development of the SSE diagnostic, SSE measurements of soot concentration and temperature were made in an atmospheric-pressure diffusion flame and compared with 2D light-attenuation soot-concentration measurements and CARS temperature measurements [11]. Results were analyzed for a variety of functional fits for $E(m)$ and it was determined that an $E(m)$ function independent of wavelength (i.e., $E(m)$ independent of wavelength) showed the best agreement [11]. It was also shown that a change in slope from constant $E(m)$ to a linear function for $E(m)$ that increased at a rate of 40%/μm resulted in a 50 K increase in measured temperature (i.e., $<3\%$ on a measured temperature of 1700 K)

and a 30% decrease in the estimated soot concentration [11]. The soot concentration varies inversely with the absolute magnitude of $E(m)$. Therefore, the soot volume fraction is much more sensitive to the selection of $E(m)$ than is the temperature. For the present measurements, a constant $E(m)$ function with a magnitude of 0.274 is assumed. This is consistent with the results of Krishnan et al. [15] and the previous measurements with methane flames [6].

Modeling of the flame emission using the methods described in [11] showed that attenuation of emission by soot introduces only a small error into the measurements (i.e., $<2\%$) for even the highest soot loadings observed in this flame. This result may seem surprising considering that soot volume fractions of 80 ppm have been measured in this flame; however, light attenuation is a function of the product of the soot concentration and the absorption path length. Although soot concentrations are a factor of 10 larger than those observed in the familiar atmospheric flames, e.g., [14,16], the flame diameter is much smaller and decreases with increasing pressure. A more detailed discussion of the subject can be found in [26].

Reliable measurements with SSE were only possible in the radial region around the emission intensity annulus as noted before [6]. The total uncertainty of the temperature and soot volume fraction measurements is dominated by the uncertainty of the soot refractive index as discussed above. The total uncertainty in temperature was estimated as 3.5% and the total uncertainty in soot volume fraction as 40% with a 95% confidence interval [17,18]. Total uncertainty of the soot volume fraction measurements of LOSA method was estimated as 20–30% with a 95% confidence interval, similar to previous error assessments [6].

4. Conclusions

Spectral soot emission was used to measure radially resolved soot volume fraction and soot temperature as a function of pressure in coflow propane–air laminar diffusion flames. Additional soot volume fraction measurements were made using line-of-sight light attenuation at certain heights and pressures to complement the SSE measurements. The visible flame height marked by the presence of soot did not change significantly between 0.2 and 0.73 MPa. Between 0.2 and 0.73 MPa pressure, the cross-sectional area of the flame (measured from the radius defined by the outer edges of the sooting region at each measurement height) showed an inverse dependence on pressure. Peak carbon conversion to soot, defined as the percentage of fuel's carbon content converted to soot, followed a power-law dependence on pressure, where the pressure exponent is about 1.1 for pressures between 0.2 and 0.73 MPa. This is slightly higher than the exponent reported for methane diffusion flames. Soot temperature measurements showed that the overall temperature decreases with increasing pressure; however, the temperature gradients increases with increasing pressure.

Acknowledgments

We thank G.J. Smallwood for allowing us to use the high-pressure facilities at the National Research Council Canada while the UTIAS high-pressure combustion chamber was being built. Advice given by D.R. Snelling on optical matters and assistance of M.F. Baksh with the experimental setup are gratefully acknowledged. Funding for this work has been provided by Natural Sciences and Engineering Research Council (NSERC).

References

[1] A.V. Krestinin, Combust. Flame 121 (2000) 513–524.
[2] G.M. Faeth, in: H.D. Ross (Ed.), Microgravity Combustion, Academic Press, 2001, p. 83.
[3] J.B. Moss, in: G. Cox (Ed.), Combustion Fundamentals of Fire, Academic Press, 1995.
[4] A. Cavaliere, R. Ragucci, Prog. Energy Combust. Sci. 27 (2001) 547–585.
[5] I.M. Miller, H.G. Maahs, NASA Technical Paper TN D-8407 (1977).
[6] K.A. Thomson, Ö.L. Gülder, E.J. Weckman, R.A. Fraser, G.J. Smallwood, D.R. Snelling, Combust. Flame 140 (2005) 222–232.
[7] W.L. Flower, C.T. Bowman, Proc. Combust. Inst. 21 (1986) 1115–1124.
[8] W. Lee, Y.D. Na, JSME Int. J. Ser. B 43 (4) (2000) 550–555.
[9] L.L. McCrain, W.L. Roberts, Combust. Flame 140 (2005) 60–69.
[10] F.G. Roper, Combust. Flame 29 (3) (1977) 219–226.
[11] D.R. Snelling, K.A. Thomson, G.J. Smallwood, Ö.L. Gülder, E.J. Weckman, R.A. Fraser, AIAA J. 40 (9) (2002) 1789–1795.
[12] C.J. Dasch, Appl. Opt. 31 (8) (1992) 1146–1152.
[13] S.S. Krishnan, K.-C. Lin, G.M. Faeth, J. Heat Transfer 122 (2000) 517–524.
[14] D.R. Snelling, K.A. Thomson, G.J. Smallwood, Ö.L. Gülder, Appl. Opt. 38 (12) (1999) 2478–2485.
[15] I. Glassman, Proc. Combust. Inst. 27 (1998) 1589–1596.
[16] R.J. Santoro, T.T. Yeh, J.J. Horvath, H.G. Semerjian, Combust. Sci. Technol. 53 (2–3) (1987) 89–115.
[17] K.A. Thomson, Ph.D. thesis, Mechanical Engineering, University of Waterloo, Canada, 2005.
[18] D.S. Bento, M.A.Sc. thesis, UTIAS, University of Toronto, Canada, 2005.

[19] W.L. Flower, Combust. Flame 77 (1989) 279–293.
[20] S.C. Li, C.L. Tien, Proc. Combust. Inst. 18 (1981) 1159–1166.
[21] T.T. Charalampopoulos, H. Chang, B. Stagg, Fuel 68 (1989) 1173–1179.
[22] C.M. Sorenson, Aerosol Sci. Technol. 35 (2) (2001) 648–687.
[23] T.L. Farias, M.G. Carvalho, Ö.Ü. Köylü, G.M. Faeth, J. Heat Transfer 117 (1) (1995) 152–159.
[24] G.M. Faeth, Ö.Ü. Köylü, Combust. Sci. Technol. 108 (4–6) (1995) 207–229.
[25] T.L. Farias, Ö.Ü. Köylü, M.G. Carvalho, Appl. Opt. 35 (33) (1996) 6560–6567.
[26] J.J. Murphy, C.R. Shaddix, Combust. Flame 143 (2005) 1–10.